CHEMISTRY OF MATERIALS

Article

pubs.acs.org/cm

Transversally Extended Laser Plasmonic Welding for Oxidation-Free Copper Fabrication toward High-Fidelity Optoelectronics

Jung Hwan Park,[†,§] Sunho Jeong,[*,‡,§] Eun Jung Lee,[‡] Sun Sook Lee,[‡] Jae Young Seok,[†] Minyang Yang,[*,†] Youngmin Choi,[*,‡] and Bongchul Kang[*,⊥]

[†]Department of Mechanical Engineering, Korea Advanced Institute of Science and Technology (KAIST), 291 Daehak-ro, Yuseong-gu, Daejeon 305-701, Republic of Korea

[‡]Division of Advanced Materials, Korea Research Institute of Chemical Technology (KRICT), 141 Gajeong-ro, Yuseong-gu, Daejeon 305-600, Republic of Korea

[⊥]Department of Mechanical System Engineering, Kumoh National Institute of Technology, 61 Daehak-ro (yangho-dong), Gumi, Gyeongbuk 730-701, Republic of Korea

Supporting Information

ABSTRACT: Laser direct processing is a promising approach for future flexible electronics because it enables easy, rapid, scalable, and low-temperature fabrication without using expensive equipment and toxic material. However, its application for nanomaterials with high chemical susceptibility, such as representatively Cu, is limited because severe oxidation occurs under ambient conditions. Here, we report the methodology of a transversally extended laser plasmonic welding process, which outstandingly improves the electrical performance of a Cu conductor (4.6 $\mu\Omega$·cm) by involving the spatially concurrent laser absorption to the surface oxide-free Cu nanoparticles (NPs). Physical/chemical properties of fabricated Cu conductors are fully analyzed in perspectives of the mechanism based on the thermo-physical-chemical interactions between photon energy and pure Cu NPs. The resultant Cu conductors showed an excellent durability in terms of bending and adhesion. Furthermore, we successfully demonstrated a single layer Cu-mesh-based touch screen panel (TSP) on thermally sensitive polymer film as a breakthrough of typical metal oxide-based transparent touch sensors. The Cu metal mesh exhibited high transmittance (95%) and low sheet resistance (30 Ω/square). This self-capacitance type and multitouchable TSP operated with a fast response, high sensitivity, and durability.

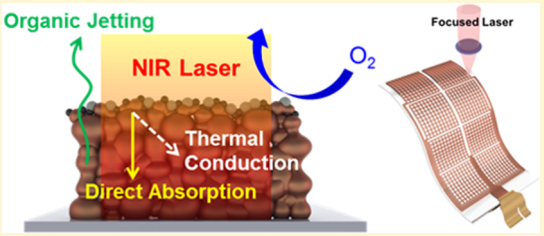

INTRODUCTION

The characteristic physical properties of Cu, coupled with its low-cost, has led to much effort over the past decade to use it to replace Ag as the active element in highly conductive, cost-effective systems for a variety of optoelectronic applications such as touch screens, organic light emitting diode displays, transparent heaters, and photovoltaics.[1−5] However, a critical impediment for its practical applications is that the Cu phase readily oxidizes upon exposure to air, such that sophisticated processing technologies are indispensable for producing device-applicable Cu-based conductors. The standard reduction potential of Cu (0.34 V) is much lower than those of Au (1.52 V) and Ag (0.8 V), the other metals with similar electrical properties.[6] To date, Cu electrode-based devices have been fabricated predominantly by vacuum deposition techniques and electro/electroless platings with a photolithography process for forming patterned structures of a specific geometry. Photolithographic techniques are extremely well developed, and are applicable even down to sub-micrometer resolution. However, they are quite costly due to the need for expensive facilities, the involvement of a number of sequential steps, and the fact that they are only suitable for rigid substrates rather than flexible plastic ones, which limits their use in the highly productive roll-to-roll processes.

Solution-based processes, based on metallic colloidal nanoparticles (NPs), combined with various printing techniques, are recognized as one of the most promising methodologies for resolving such practical issues.[7−12] However, surface-to-bulk oxidation in nanosized Cu NPs is poorly controllable due to the high surface area of spherical particles with dimensions of a few tens of nanometer. Oxidation can be suppressed by introducing a thin oxide or a surface-capping layer for passivating the thermodynamically active Cu NP surface; however, the precise control of both thickness and uniformity of the shell layer is highly demanding because of difficulties in adjusting the surface chemical reactions on the nanometer scale.[13−15] In addition, an inert gas or a high-vacuum environment is necessary to prevent the thermal oxidation of the Cu NPs during the thermal annealing at elevated temperatures (typically >250 °C), needed to produce the structural densification.[16−19] This reduces the

Received: January 5, 2016
Revised: May 30, 2016
Published: May 31, 2016

Downloaded via UNIV OF CALIFORNIA BERKELEY on March 18, 2019 at 22:01:46 (UTC).
See https://pubs.acs.org/sharingguidelines for options on how to legitimately share published articles.

© 2016 American Chemical Society

DOI: 10.1021/acs.chemmater.6b00013
Chem. Mater. 2016, 28, 4151−4159

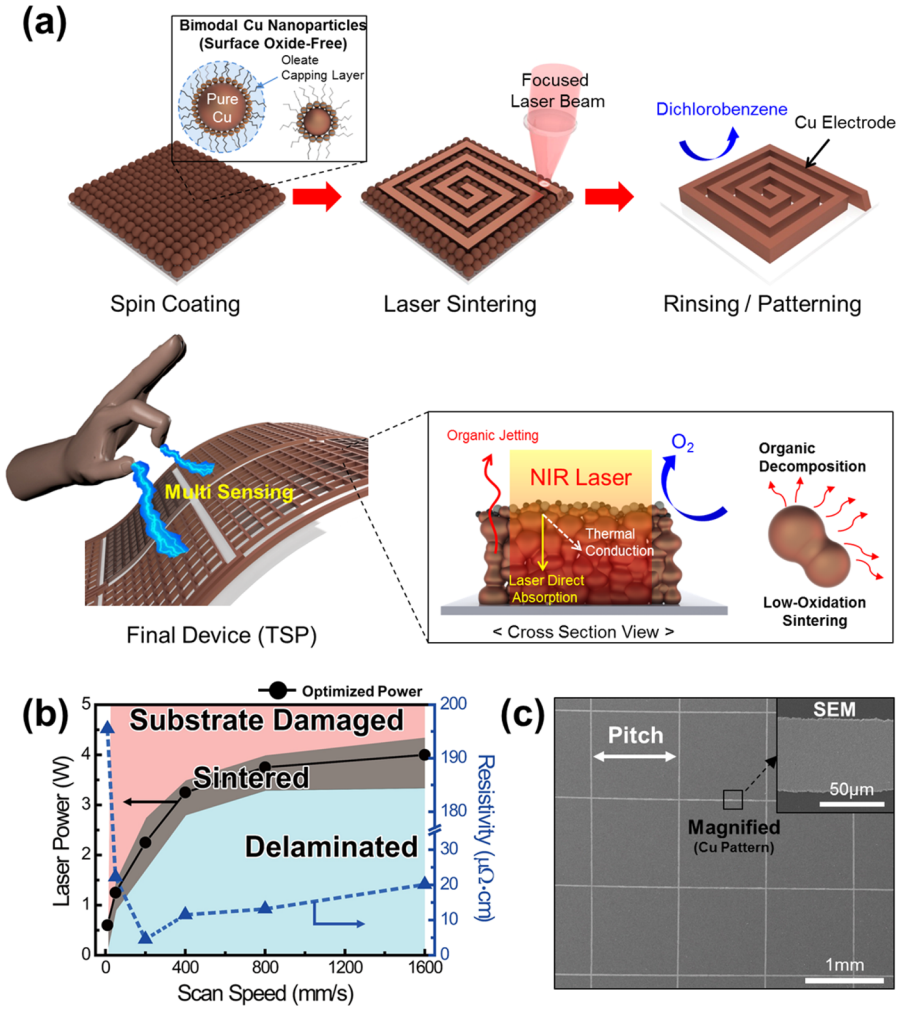

Figure 1. (a) Schematic illustrations showing the patterning process using a TLP welding for Cu NP assemblies and its final device, (b) NIR-laser processing condition when the ablation, welding (optimized; minimum resistivity), and delamination were occurred (left *Y*-axis), and the measured minimum resistivity (right *Y*-axis), (c) SEM images of fabricated Cu conductor.

main economic advantage of the low cost of Cu materials over the environmentally stable Ag.

Laser-based direct welding methodology has been developed as an alternative to conventional thermal annealing. In this case, the energy for triggering the structural evolution of NP films is supplied by high energetic photons. Noble metal (Ag and Au) NP-based electrodes have been shown to be easily applicable to this laser sintering process, even using low-cost, vulnerable plastic substrates.[20−26] However, until now, the facile processability of laser-annealed Cu electrodes under ambient atmosphere has not been demonstrated;[27−29] the demonstration of the electrically active Cu electrodes was limited to an inexpensive polyimide (PI) plastic film and a rigid glass substrate, due to the lack of in-depth studies of physical/chemical interaction of photons with the easily oxidizable Cu phase.[28,29] In previous studies, a laser source has been employed, with a wavelength (typically below 550 nm) that allows the surface plasmon resonance (SPR), for improving the degree of absorption.[20−25,27−30] The application of laser welding, intensified via the SPR effect, has been demonstrated for the cases of the noble metal, Ag and Au NPs that do not undergo significant oxidation.[20−25,30] However, for the easily oxidizable Cu NPs, the photon energy, localized on the top surface of the particle layer, could give rise to adverse effects through the selective intensive absorption of laser energy. No methodology for producing a transversally extended laser plasmonic (TLP) welding for fabricating device-applicable, high-performance Cu electrodes under ambient atmospheres has yet been presented. Further, no in-depth interpretation has been given for the evolution of the chemical structure in Cu NP assemblies under irradiation with highly energetic photons.

In this study, we provide the first report of the TLP welding process of Cu NP assemblies to fabricate high-quality, cost-effective Cu conductors in air on various substrates, including low-cost polyethylene terephthalate (PET). This includes a detailed study on the mechanism of interaction between Cu NPs and photons from a laser. This has not previously been reported, mainly because of the chemical structural complexity of systems, with a Cu NP core surrounded by a surface oxide layer and organic capping molecules. We provide a simplified, but comprehensive, investigation of TLP fusing process using surface oxide-free Cu NPs, and elucidate the factors determining their chemical/electrical properties. This combinatorial approach, based on the spatially concurrent laser absorption and surface oxide-free Cu NPs, leads to highly conductive, directly writable Cu conductors, suitable for application for touch screen panel (TSP).

DOI: 10.1021/acs.chemmater.6b00013
Chem. Mater. 2016, 28, 4151−4159

RESULTS AND DISCUSSION

The surface oxide-free Cu NPs were synthesized as described previously.[19,31] Briefly, Cu ions, derived from the Cu acetate salt, were thermo-chemically reduced, using phenylhydrazine, in an octylamine reaction medium, at an elevated temperature of 180 °C in the presence of oleic acid as a capping molecule. As shown in Figure S1, the resulting Cu NPs were spherical in shape, and showed a bimodal particle size distribution (≤110 nm), surrounded by an oxide-free, carboxylate-based shell layer. Films were deposited on various substrates by spin-coating an ink containing the Cu NPs. When a thermal annealing was carried out under an inert atmosphere as a control experiment, the electrical conductivity started to evolve after annealing at 250 °C, and exhibited bulk-like resistivity, approaching 5.9 $\mu\Omega$·cm, after annealing at 300 °C (Figure S2). When a thermal annealing was carried out in air, black-colored, fully oxidized films were generated, losing the inherent electrical properties of the metallic Cu phase.

The optical characteristic of Cu NPs was analyzed for an effective fabrication of Cu conductors by a laser welding method. As shown in Figure S3, the extinction coefficient value of Cu NP film at near-infrared (NIR) spectrum is much lower than that of the SPR region (near 560 nm in wavelength), which is supported by previous reports.[32,33] On the basis of this measurement result, the theoretical absorption depth for wavelength from 400 to 1070 nm was investigated according to the fundamentals of classical electromagnetic theory as shown in Figure S4.[34] The calculated absorption length at the NIR region (at a wavelength of 1064 nm) is approximately 25 times longer than that of the SPR region (at a wavelength of 532 nm). This difference of absorption depth can generate a considerable distinction between TLP welding and conventional surface laser sintering in terms of degree of absorption and welding mechanism. For the SPR-oriented laser welding, the photon energy is localized only at the surface, and then the absorbed energy is indirectly delivered to the bottom Cu NPs by a thermal conduction. However, for the TLP fusing process, the transversally uniform heat is directly generated, causing homogeneous densification of Cu NP film. The spatially concurrent and direct laser absorption is effective to suppress the oxidation of Cu electrodes in air as it is not involved with a provision of excessive energy for sintering the Cu NPs down to a bottom layer. Therefore, a NIR-laser (1064 nm wavelength) was employed to ensure that the photons do not trigger any SPR effect of Cu NPs, but primarily lead vertically extended welding. Highly purified Cu NP was used as a chemical reference for simultaneously monitoring the oxidation behavior of the Cu NPs (without the ambiguous involvement of inherent surface oxide layer), as well as the decomposition of residual organics. When the NIR-laser is irradiated onto the Cu NPs, a vertically homogeneous thermal energy is generated deep through the bottom by a long absorption depth, which enables a transversally extended welding of Cu NPs for high performance conductor. The part of the Cu particulate film that does not undergo laser sintering was removed by a simple washing technique in dichlorobenzene (DCB) for patterning the Cu conductors in a direct-writable way.

The laser welding parameters, such as a laser scan rate and a power, give rise to a critical influence on interparticular densification between neighboring NPs. These parameters are interrelated, as the energy input per unit volume is determined by the relationship between a scan rate and a power at a given wavelength. The electrical resistivities of laser-irradiated Cu nanoparticulate films were measured by varying these parameters to determine the dependence of sintering behavior on input laser energy. Figure 1b shows the optimized laser power as a function of scan speed, from 10 to 1600 mm·s^{-1}. All films were prepared on a glass substrate with a thickness of 200 nm. The evolution of electrically resistive Cu films out of this scan speed range is attributable to an insufficient supply of photon energy above 1600 mm·s^{-1} and generation of a distinctive oxidized layer below 10 mm·s^{-1}. The laser power was adjusted for each scan rate to prevent unwanted morphological destruction, such as ablation or delamination. When the laser power was too low at a certain scan rate, either the resistivity could not be recorded because of delamination of patterned structures from substrates during washing, or the resistivity was poor due to insufficient agglomerated grain-growth between Cu NPs. When the laser power was above the optimum range, the Cu NPs underwent thermal damage, for instance, formation of an ablated morphology, substrate damage, and/or oxidation. Interestingly, the dependence of optimized laser power (showing the minimum electrical resistivity) on scan speed is not linear, but rather shows a parabolic relationship for scan speeds over 200 mm·s^{-1}; this indicates that the required energy input for triggering an efficient fusing process does not have a linear relationship with the scan rate and cannot be determined by a simple numerical calculation.

Figure 1b shows the dependence of the evolution of resistivity on the scan rate in the range of 10 to 1600 mm·s^{-1}, under conditions with optimized laser power. The most resistive electrode, with a resistivity value of 195.5 $\mu\Omega$·cm, was developed with a low scan rate of 10 mm·s^{-1}. The resistivity gradually improved to the value of 4.6 $\mu\Omega$·cm, close to that of bulk pure Cu phase, as the scan rate increased up to 200 mm·s^{-1}. Then, with scan rates above 200 mm·s^{-1}, the resistivity increased as a function of scan speed. Considering the limited laser power at high scan rates, it is likely that the structural densification by agglomeration would be suppressed as the scan speed increased above 200 mm·s^{-1}, impeding the evolution of electrically conductive pathways. The degree of densification could be characterized qualitatively by comparing how well the welded morphology between neighboring NPs was generated. As can be seen in Figure S5, the microstructural transformation toward a bulk-like morphology led to distinctive compartmentalization at the boundary condition of 200 mm·s^{-1}. However, the morphological properties appeared to be almost identical when the scan speed was below 200 mm·s^{-1}, showing fully fused structures, despite huge differences in resistivity, from 4.6 to 195.5 $\mu\Omega$·cm. This implies that complicated chemical structural variations, resulting from the thermal or photochemical decomposition of organic residues and the subsequent structural oxidation, were produced in a laser welding process, together with the instant structural transformations induced by the high intensity photons.

To clarify both the evolution of the oxidation processes and the decomposition behavior of organic moieties, X-ray photoelectron spectroscopy (XPS) analysis was carried out for the Cu films sintered with the different laser scan speeds, ranging from 10 to 1600 mm·s^{-1}. The Cu $2p_{3/2}$ spectra was recorded, and shown in Figure 2a. the subpeaks at 932.5, 932.9, 934.3, and 931.1 eV were associated with Cu, Cu_2O, CuO, and an unknown phase, respectively. Taken into consideration of the area contribution of unknown phase in Cu $2p_{3/2}$ spectra, its

DOI: 10.1021/acs.chemmater.6b00013
Chem. Mater. 2016, 28, 4151−4159

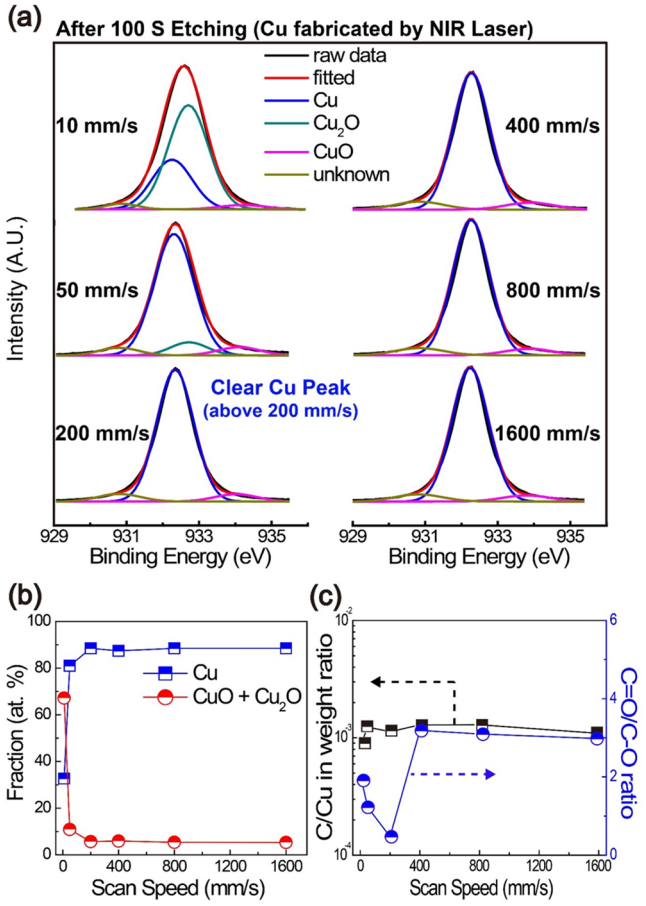

Figure 2. (a) Cu $2p_{3/2}$ XPS spectra, (b) fraction of Cu and oxide phases, obtained from Cu $2p_{3/2}$ XPS spectra, (c) ratio of carbon to Cu, and the ratio of C═O to C—O bonds in O 1s XPS spectra for NIR-laser welded Cu films under different scan rate conditions from 10 to 1600 mm·s^{-1}. For XPS analysis, all Cu films were etched for 100 s.

influence on electrical properties is almost negligible. According to a thermodynamic behavior of Cu phase, the CuO phase should be produced with a laser processing under ambient conditions. We speculate that the presence of Cu_2O phase is associated with laser-induced, photothermal oxidation, while the unknown phase is attributed to the involvement of oxygen molecules in the carboxylates anchored to the Cu NP surface. Figure 2b depicts the atomic fractions for pure Cu and oxide, CuO and Cu_2O, phases, calculated based on semiquantitative analysis using the integrated areas of each subpeak in the Cu $2p_{3/2}$ spectra. As can be seen in Figure 2b, the oxidation trend was strongly dependent on the scan speed. When this increased from 10 to 200 mm·s^{-1}, the atomic fractions of oxides decreased dramatically from 67.2 to 5.7, whereas oxidation behavior was nearly identical above 200 mm·s^{-1}. Note that the XPS spectra were acquired from surface etched films, so that the interpretation avoids problems with surface contaminant layers. Cu NPs are highly vulnerable toward oxidation because of their high surface-to-volume ratio; the Cu phase is readily converted into fully oxide phases at elevated temperatures in air, by the bulk oxidation behavior rather than self-limited surface reaction. In contrast, for bulk Cu foils, oxidation is limited to surface layers, as is commonly observed in many oxidizable bulk materials; as a consequence, the high bulk conductivities are preserved sufficiently to be usable in practical electronics applications. With the laser welding process involving NP films, the oxidation can be suppressed kinetically under ambient conditions through the ultrafast structural transformation of NP assemblies into bulk-like skeletons. Instant irradiation by very intense photons generates immediately the bulk structures, and the suppressed surface oxidation proceeds, similarly to the case of bulk Cu foils. For Cu films agglomerated with laser speeds above 200 mm·s^{-1}, the presence of small quantities of oxides can be explained through this self-limited surface oxidation in bulk-like phases. In contrast, with laser scan speeds below 200 mm·s^{-1}, the structural transformation toward bulk structures occurs slowly; thus, the bulk oxidation of Cu NPs partially take place prior to the complete densification, leaving behind the highly resistive, metal oxide structures.

Upon irradiation with high intensity photons, the removal of the organic capping layer is triggered, and the bare Cu surfaces become exposed to air. From the scan speed-dependent variation of weight ratios of C to Cu and C═O to C—O chemical bonds, the laser scan speed is also seen to affect significantly the decomposition of the organic moieties (Figure 2c). The ratios of C to Cu were obtained from the compositional analysis for C 1s and Cu 2p spectra, and the ratios of C═O to C—O chemical bonds were calculated through the area integration of each subpeak in the O 1s spectra. The deconvolutions of the O 1s spectra for all the samples are shown in Figure S6; the subpeaks positioned at 529.2, 530.2, 530.4, and 531.7 eV are due to the chemical moieties CuO, C—O, Cu_2O, and C═O, respectively, whereas the unknown phases, similarly observed for the Cu $2p_{3/2}$ spectra, are located at 532.9 and 534.5 eV. The C/Cu weight ratios did not vary, and had negligible values of ~10^{-3} for all samples, regardless of scan speed conditions; this implies that laser irradiation, even on time scales corresponding to scan rates of 0.1−0.0006 s·mm^{-1}, effectively removes the aliphatic organic moieties. However, for the carboxylates, having C—O and C═O groups through mixed bidentate and monodentate bonding characteristics,[19] the C═O/C—O ratios varied with scan speeds. In general, more energy is needed for decomposing C═O than C—O chemical bonds; thus, the ratio of C═O to C—O represents how efficiently the decomposition of carboxylates proceeds during the instant irradiation with intense photons. The ratio of oxygen to Cu does not clearly represent the degree of carboxylate decomposition, because of the contribution of the oxide phases on oxygen content. Under the scan speed conditions ranging from 10 to 200 mm·s^{-1}, the ratio of C═O to C—O decreased almost linearly from 1.89 to 0.47, which indicates that the decomposition of carboxylates was gradually activated with increasing scan speeds, up to 200 mm·s^{-1}. As discussed above, using laser irradiation with scan speeds below 200 mm·s^{-1}, the total energy input was almost identical. It is postulated that the formation of oxide phases at low scan speeds interrupts the decomposition of carboxylates due to inefficient absorption of photons by the oxides, which provides another plausible reason for the high resistivities observed for Cu films sintered below scan speeds of 200 mm·s^{-1}. Above 200 mm·s^{-1}, the C═O/C—O ratios increased abruptly to the value of ~3. Under these conditions, the laser power was limited to avoid Cu film ablation, which would restrict the energy input inside Cu NPs assemblies, resulting in a reduced decomposition of organic moieties. This chemical structure evolution, together with formation of less dense morphologies, can be related to the slightly higher resistivities for the Cu films sintered with scan

DOI: 10.1021/acs.chemmater.6b00013
Chem. Mater. 2016, 28, 4151−4159

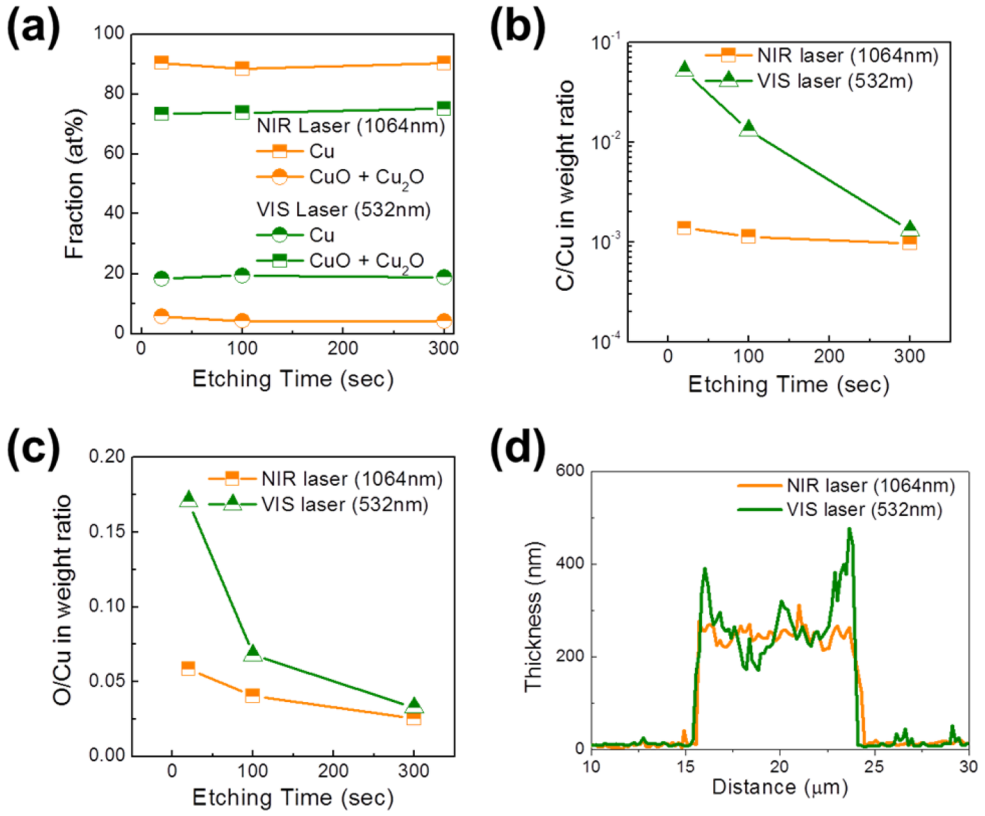

Figure 3. (a) Fractions of Cu and oxide phases, obtained from Cu $2p_{3/2}$ XPS spectra, (b) ratio of carbon to Cu, and (c) ratio of oxygen to Cu as a function of etching time for both NIR-laser and VIS-laser welded Cu films. The weight ratios of C to Cu and O to Cu as a function of the etching time for both laser welded Cu films, were calculated based on the compositional analysis for C, O, and Cu spectra. (d) AFM morphological profile for NIR-laser and VIS-laser welded Cu electrodes.

speeds over 200 mm·s^{-1}. On the basis of the chemical information obtained from XPS analysis, electrical resistivities, and morphological evolutions, it is speculated that there is a complicated relation between the irradiation of highly energetic photons and the formation of oxide phase, the decomposition of organic moieties, and structural densification. However, the oxide phase formation is postulated, overwhelmingly, to be the dominant factor in the development of the highly conductive Cu frameworks, based on the analytical results for Cu films sintered at scan speeds of 10−50 and 400−1600 mm·s^{-1}. This fundamental result suggests that optimization of processing parameters in laser fusing methodologies should be considered to suppress effectively the oxidation to generate highly conductive, fine-patterned Cu architectures. We can also conclude that the scan rate of 200 mm·s^{-1} is optimal for the TLP welding in Cu NP assemblies; this is fast enough for fabricating micrometer-sized electrodes for use in high-density electronic devices. Figure 1c shows scanning electron microscopy imaging (SEM) of Cu conductor fabricated at a scan rate of 200 mm·s^{-1}.

The critical influence of laser irradiation wavelength on the Cu NP agglomeration behavior was also studied to clarify the importance of the TLP welding mechanism over the surficial laser plasmonic (SLP) fusing process as a counterpart. Figure 3a shows the results of the XPS analyses of NIR (1064 nm) and visible (532 nm) laser-patterned Cu films. During both laser experiments, the laser scan rate and the film thickness were 200 mm·s^{-1} and 200 nm, respectively. The laser power for the VIS-laser was adjusted to obtain the optimal processing conditions (Figure S7). The atomic fractions of Cu and oxide phases were analyzed across the film thickness by integration of the area of each subpeak in the Cu $2p_{3/2}$ spectra. All Cu $2p_{3/2}$ spectra were acquired after etching from 20 to 300 s (Figure S8), and the positions of each subpeak were identical to those in the spectra in Figure 2a. As shown in Figure 3a, both Cu films showed uniform compositional distribution in their overall vertical positions. However, significant differences are observed in the degree of oxidation, depending on the laser source, with a much higher oxide fraction in the VIS-laser-welded Cu films. This is associated with the enhanced heating by SPR-based VIS-laser fusing, as the chemical oxidation of the Cu phase depends predominantly on the thermal activity of the ambient oxygen.

From Figure 3b,c, organic residues were present in greater amounts in the top surface layer of VIS-laser welded films, compared with that of the Cu films welded using a NIR-laser. It was also found that although the composition of C and O with respect to Cu did not vary with the NIR-laser processed Cu films, the C/Cu and O/Cu ratios decreased drastically on moving away from the top surface in VIS-laser processed ones. In conventional thermal annealing, the diffusion of surface atoms in metal NPs is triggered, and can be processed for a prolonged time, with the gradual thermal decomposition of organic moieties; this results in highly pure metallic conductors, with small amounts of organic impurities. In contrast, when highly energetic photons are used for irradiation in the laser process, both densification of a particle-assembled structure and decomposition of organic moieties take place on a kinetically controlled time scale. For the case of the SLP welding based VIS-laser process, the degree of absorption is dramatically enhanced in the surface layer; thus, the kinetics for the welding

DOI: 10.1021/acs.chemmater.6b00013
Chem. Mater. 2016, 28, 4151−4159

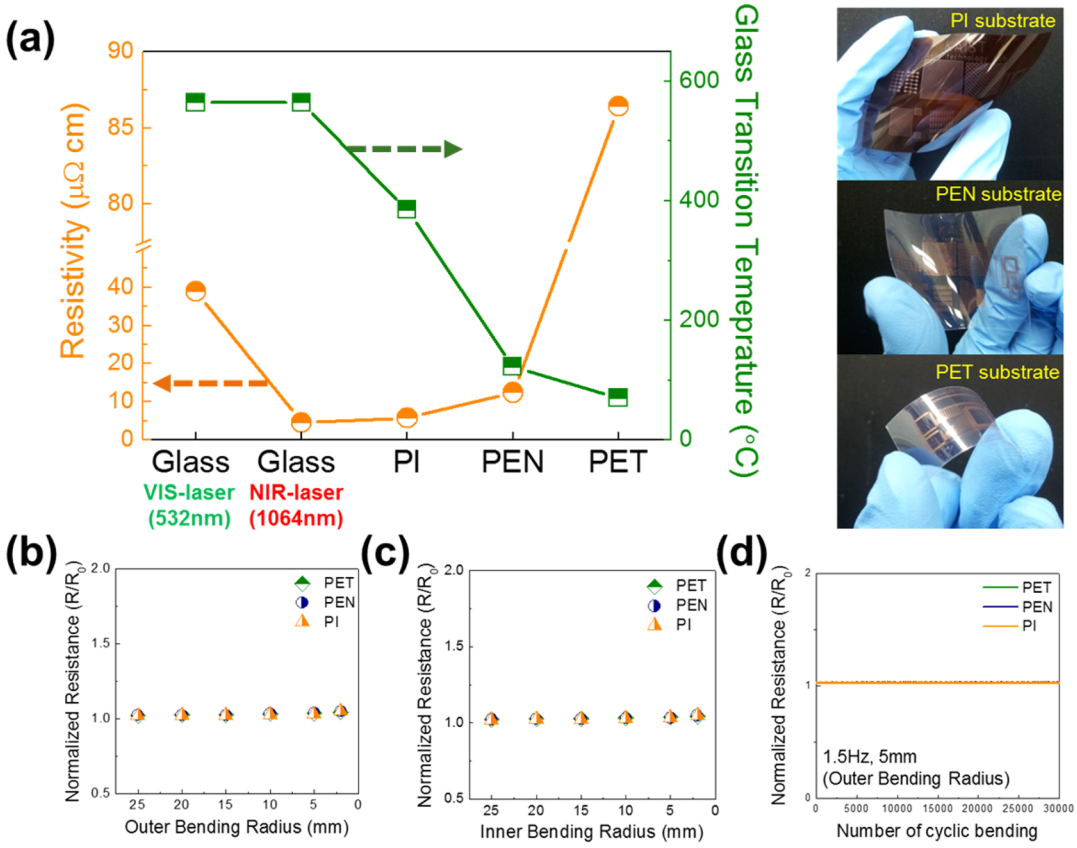

Figure 4. (a) Minimum resistivities obtained from Cu electrodes on glass, PI, PEN, and PET substrates. The Cu electrodes on PI, PEN, and PET substrates were formed using a NIR-laser welding process, and the Cu electrodes on glass substrate were fabricated using both VIS-and NIR-laser welding process. (b, c) Variation of normalized resistance for NIR-laser welded Cu electrodes on PI, PEN, and PET substrates, as a function of outer- and inner-bending radius. (d) Cycling bending test for NIR-laser welded Cu electrodes on PI, PEN, and PET substrates. The bending radius was 5 mm and the frequency was 1.5 Hz.

process are greatly accelerated in the localized surface region, resulting in even less efficient evaporation of decomposed organic moieties, and the spatial presence of organic impurities in a fully densified film-like structure. The absorption/dissipation of photon energy from the VIS-laser is localized in a limited surface layer, such that internal lower layers will not absorb directly the energy from the laser irradiation. This is supported by the morphological results, which showed that interparticular grain growth inside internal lower layers did not occur to any sufficient extent through the indirect input of energy by thermal conduction from the surface (Figure S9). When the laser power increased up to the level of the ablation process, such vertical inhomogeneities evolved with VIS-laser fused Cu films; this indicates that the incomplete fusion is not caused by the insufficient supply of laser power at a given scan rate. Below the surface layer, interparticular grain growth between neighboring NPs occurs with the indirect transfer of thermal energy, providing enough time for evaporating decomposed impurities, as in the case of the NIR-laser process. This agrees well with the fact that the ratios of both C/Cu and O/Cu are almost identical for VIS- and NIR-laser processed Cu films after etching for 300 s. This evidently inhomogeneous chemical structure has not been previously reported for Ag NP-based films processed with a VIS-laser. The melting points of pure bulk Ag and Cu phases are 921 and 1074 °C, respectively, and the size (40−110 nm) of Cu NPs used in this study is much larger than that (5−20 nm) of Ag NPs commonly used in other reports.[20] It becomes more demanding to control the critical surface oxidation as the size of Cu NP decreases on a nanoscale. The input energy for the complete film-like structure should, thus, be higher for the case of Cu NPs; vertical inhomogeneities in VIS-laser processed films would be significantly developed for Cu NP-based films than for the easily sintered Ag NPs.

The resistivity, 38.9 $\mu\Omega$·cm, of the VIS-laser processed Cu film was higher, by a factor of 8.5, than that of the corresponding film processed using the NIR-laser. This was due to further oxidation in VIS-laser welded Cu NPs, the insufficient densification of bottom Cu NPs owing to poor, indirect energy transfer, and the incomplete decomposition/evaporation of organic residues. The use of laser with a wavelength in a low absorption region allows for the homogeneous densification of Cu NPs in the transverse direction without a severe oxidation, as the laser is capable of penetrating deeper and mildly into NP assemblies. This volumetrically concurrent laser absorption also has a positive effect on the morphological characteristic of resulting patterns (Figure 3d).[35,36]

All the aforementioned experimental results were based on a rigid glass substrate to exclude factors resulting from more vulnerable polymer substrates in monitoring the laser-induced welding behaviors. As an extension of this, to extend the applicability to cost-effective polymeric supports, the plastic substrates including PI, polyethylene naphthalate (PEN), and PET were tested with optimized processing conditions. For plastic substrates, the thickness of Cu NP films was slightly

DOI: 10.1021/acs.chemmater.6b00013
Chem. Mater. 2016, 28, 4151−4159

higher than that for a glass substrate to prevent the substrates from undergoing photothermal damage. The Cu NP film thicknesses on PI, PEN, and PET substrates were 450, 500, and 600 nm, respectively. It was observed that the resistivity of the film was inversely proportional to the thermal resistance of the plastic substrates (Figure 4a); if the thermal resistance of substrates becomes too poor, the laser fusing process would not occur fully using the optimized level of laser power. However, the resistivity values obtained from the PI and PEN films were comparable to that for Cu NP-based electrodes obtained by conventional thermal annealing under inert atmosphere, and those for electrodes consisting of noble metal NPs.[37−40] Although the Cu electrodes fabricated on a PET film exhibited a relatively high resistivity, this might still be a valuable result, as it is challenging to generate conductive Cu architectures on the extremely vulnerable PET substrates. In addition, regardless of the kind of substrates used, including glass, PI, PEN, and PET, all the electrodes exhibited good adhesion properties, as confirmed by a simple tape test (Figure S10). The flexibility of NIR-laser processed Cu structures were evaluated by monitoring the resistance dependence on the bending radius, even down to 5 mm, with a repeated cycling test at a frequency of 1.5 Hz. As can be seen in Figure 4b,c, the electrical properties of the resulting Cu electrodes on PET, PEN, and PI substrates exhibited excellent durability, even under harsh bending conditions; this is postulated to result from the formation of a fully dense structure, composed mainly of highly pure, ductile metallic phase, along with good adhesion properties on the plastic substrates.

We fabricated a metal mesh-based TSP using a NIR-laser welding process for surface-oxide free Cu NPs in order to demonstrate the practical feasibility in large-area optoelectronic applications. One current issue of the TSP industries is to replace the currently used indium tin oxide (ITO) material, multilayer structures, and the photolithography process.[41] The methodology suggested in this study provides an immediate solution for fabricating an ITO-free, single layer TSP using a simple TLP welding process. A Cu mesh-based TSP was fabricated on a thermally enhanced PET film (Figure 5a). Both sensor and bezel electrodes were fabricated and structurally integrated in a single layer through a one-step laser processing. As shown in Figure 5b, fine Cu tracks with a width less than 5 μm and a pitch of 1000 μm were created in the shape of square meshes (7 mm × 7 mm), which were patterned as sensor channels of 5 × 8 arrays. For bezel electrodes, Cu conductors with a width of 60 μm and a pitch of 170 μm were laser-patterned to connect the metal mesh and flexible printed circuit board (FPCB). The Cu metal mesh exhibited uniform and good light-transmitting characteristics with average transmittance of 95% over the whole visible spectrum (400−700 nm) and a sheet resistance of 30 Ω/square (Figure S11). This self-capacitance type and multitouchable TSP operated with a high response rate, sensitivity, and durability, as illustrated in Figure 5c and Movie S1. Remarkable optoelectronic properties and performance were obtainable, even with the cost-effective Cu materials, as a result of both the low degree of oxidation and the vertically homogeneous densification, which are characteristic features of the TLP welding process. From the industrial viewpoint, this one-step fabrication of sensors and bezels is critically important for high yield production.

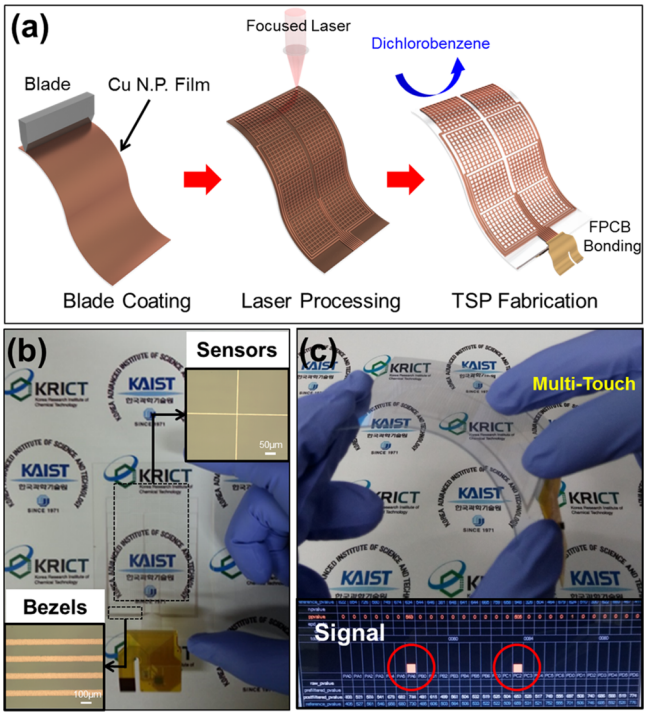

Figure 5. (a) Schematic illustrations for one-step fabrication process of Cu mesh-based TSP. (b) Optical photograph of TSP fabricated by Cu NP-TLP welding process, and microscopic images of Cu electrodes for sensors and bezels. (c) Demonstration of the self-capacitance type and multitouchable TSP fabricated through a one-step TLP welding process.

■ CONCLUSION

In summary, we have introduced a novel, facile, and scalable approach that remarkably improves the performance of laser processed Cu conductors by TLP welding using a NIR-laser of 1064 nm wavelength. Surface oxide-free Cu NPs were employed as a chemical reference for precisely monitoring the oxidation behavior and eliminating the chemical structural complexity. Laser powers and scan rates were optimized to avoid undesirable ablation, delamination, and oxidation that lead to the increase in a resistivity of fabricated Cu frameworks. The systematic chemical analysis of fabricated Cu structures allowed for the investigation of the evolution of the oxidation and decomposition/evaporation behavior of organic moieties during processing. Mechanisms obtained from the characterization of these parameters agreed well with the experimental results. The experimental results using a VIS-laser were comparatively analyzed to clarify the importance of the TLP welding process. It was confirmed that the TLP welding has outstanding advantages such as reduced amounts of oxide fractions and limited quantities of organic residues. We have presented a Cu mesh-based self-capacitance TSP on a PET film, in order to demonstrate the practical feasibility for high performance optoelectronic applications. This scientific and practical study can suggest a crucial disciplines for Cu nanomaterial laser processing, and provide an effective solution for industrial requirements.

DOI: 10.1021/acs.chemmater.6b00013
Chem. Mater. 2016, 28, 4151−4159

■ ASSOCIATED CONTENT

Supporting Information

The Supporting Information is available free of charge on the ACS Publications website at DOI: 10.1021/acs.chemmater.6b00013.

Experimental section, SEM and TEM images, resistivity measurement, extinction coefficient data, absorption depth calculation, XPS analysis, laser processing condition, photographic images, transmittance characterization (PDF).

Movie showing self-capacitance type and multitouchable TSP (AVI).

■ AUTHOR INFORMATION

Corresponding Authors

*E-mail: sjeong@krict.re.kr (S. Jeong).
*E-mail: myyang@kaist.ac.kr (M. Yang).
*E-mail: youngmin@krict.re.kr (Y. Choi).
*E-mail: kbc@kumoh.ac.kr (B. Kang).

Author Contributions

§J.H.P. and S.J. contributed equally to this work.

Notes

The authors declare no competing financial interest.

■ ACKNOWLEDGMENTS

This work was supported by the National Research Foundation (NRF) of Korea (grant code: 2014R1A1A1004048), National Research Foundation (NRF) of Korea (grant no. 2012-010307), Global Research Laboratory Program of the National Research Foundation (NRF) funded by Ministry of Science, Information and Communication Technologies and Future Planning (NRF-2015K1A1A2029679), and the Nano·Material Technology Development Program through the National Research Foundation (NRF) of Korea funded by the Ministry of Science, Information and Communication Technologies and Future Planning (NRF-2015M3A7B4050306).

■ REFERENCES

(1) Han, S.; Hong, S.; Ham, J.; Yeo, J.; Lee, J.; Kang, B.; Lee, P.; Kwon, J.; Lee, S. S.; Yang, M. Y.; et al. Fast Plasmonic Laser Nanowelding for a Cu-Nanowire Percolation Network for Flexible Transparent Conductors and Stretchable Electronics. *Adv. Mater.* **2014**, *26*, 5808−5814.

(2) Im, H. G.; Jung, S. H.; Jin, J.; Lee, D.; Lee, J.; Lee, D.; Lee, J. Y.; Kim, I. D.; Bae, B. S. Flexible Transparent Conducting Hybrid Film Using a Surface-Embedded Copper Nanowire Network: A Highly Oxidation-Resistant Copper Nanowire Electrode for Flexible Optoelectronics. *ACS Nano* **2014**, *8*, 10973−10979.

(3) Rathmell, A. R.; Bergin, S. M.; Hua, Y. L.; Li, Z. Y.; Wiley, B. J. The Growth Mechanism of Copper Nanowires and Their Properties in Flexible, Transparent Conducting Films. *Adv. Mater.* **2010**, *22*, 3558−3563.

(4) Han, S.; Hong, S.; Yeo, J.; Kim, D.; Kang, B.; Yang, M. Y.; Ko, S. H. Nanorecycling: Monolithic Integration of Copper and Copper Oxide Nanowire Network Electrode through Selective Reversible Photothermochemical Reduction. *Adv. Mater.* **2015**, *27*, 6397−6403.

(5) Won, Y.; Kim, A.; Lee, D.; Yang, W.; Woo, K.; Jeong, S.; Moon, J. Annealing-Free Fabrication of Highly Oxidation-Resistive Copper Nanowire Composite Conductors for Photovoltaics. *NPG Asia Mater.* **2014**, *6*, e105.

(6) Kang, B.; Han, S.; Kim, J.; Ko, S.; Yang, M. One-Step Fabrication of Copper Electrode by Laser-Induced Direct Local Reduction and Agglomeration of Copper Oxide Nanoparticle. *J. Phys. Chem. C* **2011**, *115*, 23664−23670.

(7) Jo, Y.; Oh, S. J.; Lee, S. S.; Seo, Y. H.; Ryu, B. H.; Moon, J.; Choi, Y.; Jeong, S. Extremely Flexible, Printable Ag Conductive Features on PET and Paper Substrates via Continuous Millisecond Photonic Sintering in a Large Area. *J. Mater. Chem. C* **2014**, *2*, 9746−9753.

(8) Hecht, D. S.; Hu, L.; Irvin, G. Emerging Transparent Electrodes Based on Thin Films of Carbon Nanotubes, Graphene, and Metallic Nanostructures. *Adv. Mater.* **2011**, *23*, 1482−1513.

(9) Kang, H.; Kitsomboonloha, R.; Jang, J.; Subramanian, V. High-Performance Printed Transistors Realized Using Femtoliter Gravure-Printed Sub-10 um Metallic Nanoparticle Patterns and Highly Uniform Polymer Dielectric and Semiconductor Layers. *Adv. Mater.* **2012**, *24*, 3065−3069.

(10) Voigt, M. M.; Guite, A.; Chung, D. Y.; Khan, R. U. A.; Campbell, A. J.; Bradley, D. D. C.; Meng, F.; Steinke, J. H. G.; Tierney, S.; McCulloch, I.; et al. Polymer Field-Effect Transistors Fabricated by the Sequential Gravure Printing of Polythiophene, Two Insulator Layers, and a Metal Ink Gate. *Adv. Funct. Mater.* **2010**, *20*, 239−246.

(11) Zheng, H.; Zheng, Y.; Liu, N.; Ai, N.; Wang, Q.; Wu, S.; Zhou, J.; Hu, D.; Yu, S.; Han, S.; et al. All-Solution Processed Polymer Light-Emitting Diode Displays. *Nat. Commun.* **2013**, *4*, 1971.

(12) Galliker, P.; Schneider, J.; Eghlidi, H.; Kress, S.; Sandoghdar, V.; Poulikakos, D. Direct Printing of Nanostructures by Electrostatic Autofocussing of Ink Nanodroplets. *Nat. Commun.* **2012**, *3*, 890.

(13) Kamyshny, A.; Magdassi, S. Conductive Nanomaterials for Printed Electronics. *Small* **2014**, *10*, 3515−3535.

(14) Jeong, S.; Song, H. C.; Lee, W. W.; Suk, H. J.; Lee, S. S.; Ahn, T.; Ka, J. W.; Choi, Y.; Yi, M. H.; Ryu, B. H. Printed Cu Source/Drain Electrode Capped by CuO Hole Injection Layer for Organic Thin Film Transistors. *J. Mater. Chem.* **2011**, *21*, 10619−10622.

(15) Jeong, S.; Song, H. C.; Lee, W. W.; Lee, S. S.; Choi, Y.; Son, W.; Kim, E. D.; Paik, C. H.; Oh, S. H.; Ryu, B. H. Stable Aqueous Based Cu Nanoparticle Ink for Printing Well-Defined Highly Conductive Features on a Plastic Substrate. *Langmuir* **2011**, *27*, 3144−3149.

(16) Kang, J. S.; Kim, H. S.; Ryu, J.; Hahn, H. T.; Jang, S.; Joung, J. W. Inkjet Printed Electronics Using Copper Nanoparticle Ink. *J. Mater. Sci.: Mater. Electron.* **2010**, *21*, 1213−1220.

(17) Jang, S.; Seo, Y.; Choi, J.; Kim, T.; Cho, J.; Kim, S.; Kim, D. Sintering of Inkjet Printed Copper Nanoparticles for Flexible Electronics. *Scr. Mater.* **2010**, *62*, 258−261.

(18) Lee, Y.; Choi, J. R.; Lee, K. J.; Stott, N. E.; Kim, D. Large-Scale Synthesis of Copper Nanoparticles by Chemically Controlled Reduction for Applications of Inkjet-Printed Electronics. *Nanotechnology* **2008**, *19*, 415604−415610.

(19) Jeong, S.; Lee, S. H.; Jo, Y.; Lee, S. S.; Seo, Y. H.; Ahn, B. W.; Kim, G.; Jang, G. E.; Park, J. U.; Ryu, B. H.; et al. Air-Stable, Surface-Oxide Free Cu Nanoparticles for Highly Conductive Cu Ink and Their Application to Printed Graphene Transistors. *J. Mater. Chem. C* **2013**, *1*, 2704−2710.

(20) Hong, S.; Yeo, J.; Kim, G.; Kim, D.; Lee, H.; Kwon, J.; Lee, H.; Lee, P.; Ko, S. H. Nonvacuum, Maskless Fabrication of a Flexible Metal Grid Transparent Conductor by Low-Temperature Selective Laser Sintering of Nanoparticle Ink. *ACS Nano* **2013**, *7*, 5024−5031.

(21) Watanabe, A.; Kobayashi, Y.; Konno, M.; Yamada, S.; Miwa, T. Direct Drawing of Ag Microwiring by Laser-Induced Pyrolysis of Film Prepared from Liquid-Dispersed Metal Nanoparticles. *Jpn. J. Appl. Phys., Part 2* **2005**, *44*, L740−L742.

(22) Chung, J.; Ko, S.; Bieri, N. R.; Grigoropoulos, C. P.; Poulikakos, D. Conductor Microstructures by Laser Curing of Printed Gold Nanoparticle Ink. *Appl. Phys. Lett.* **2004**, *84*, 801−803.

(23) Lee, H.; Hong, S.; Kwon, J.; Suh, Y. D.; Lee, J.; Moon, H.; Yeo, J.; Ko, S. H. All-Solid-State Flexible Supercapacitors by Fast Laser Annealing of Printed Metal Nanoparticle Layers. *J. Mater. Chem. A* **2015**, *3*, 8339−8345.

(24) Yeo, J.; Kim, G.; Hong, S.; Kim, M. S.; Kim, D.; Lee, J.; Lee, H. B.; Kwon, J.; Suh, Y. D.; Kang, H. W.; et al. Flexible Supercapacitor Fabrication by Room Temperature Rapid Laser Processing of Roll-to-Roll Printed Metal Nanoparticle Ink for Wearable Electronics Application. *J. Power Sources* **2014**, *246*, 562−568.

DOI: 10.1021/acs.chemmater.6b00013
Chem. Mater. 2016, 28, 4151−4159

(25) Yeo, J.; Hong, S.; Lee, D.; Hotz, N.; Lee, M. T.; Grigoropoulos, C. P.; Ko, S. H. Next Generation Non-Vacuum, Maskless, Low Temperature Nanoparticle Ink Laser Digital Direct Metal Patterning for a Large Area Flexible Electronics. *PLoS One* **2012**, *7*, e42315.
(26) Son, Y.; Yeo, J.; Moon, H.; Lim, T. W.; Hong, S.; Nam, K. H.; Yoo, S.; Grigoropoulos, C. P.; Yang, D. Y.; Ko, S. H. Nanoscale Electronics: Digital Fabrication by Direct Femtosecond Laser Processing of Metal Nanoparticles. *Adv. Mater.* **2011**, *23*, 3176−3181.
(27) Qin, G.; Watanabe, A.; Tsukamoto, H.; Yonezawa, T. Copper Film Prepared from Copper Fine Particle Paste by Laser Sintering at Room Temperature: Influences of Sintering Atmosphere on the Morphology and Resistivity. *Jpn. J. Appl. Phys.* **2014**, *53*, 096501.
(28) Joo, M.; Lee, B.; Jeong, S.; Lee, M. Laser Sintering of Cu Paste Film Printed on Polyimide Substrate. *Appl. Surf. Sci.* **2011**, *258*, 521−524.
(29) Zenou, M.; Ermak, O.; Saar, A.; Kotler, Z. Laser Sintering of Copper Nanoparticles. *J. Phys. D: Appl. Phys.* **2014**, *47*, 025501.
(30) An, K.; Hong, S.; Han, S.; Lee, H.; Yeo, J.; Ko, S. H. Selective Sintering of Metal Nanoparticle Ink for Maskless Fabrication of an Electrode Micropattern Using a Spatially Modulated Laser Beam by a Digital Micromirror Device. *ACS Appl. Mater. Interfaces* **2014**, *6*, 2786−2790.
(31) Oh, S. J.; Jo, Y.; Lee, E. J.; Lee, S. S.; Kang, Y. H.; Jeon, H. J.; Cho, S. Y.; Park, J. S.; Seo, Y. H.; Ryu, B. H.; et al. Ambient Atmosphere-Processable, Printable Cu Electrodes for Flexible Device Applications: Structural Welding on a Millisecond Timescale of Surface Oxide-Free Cu Nanoparticles. *Nanoscale* **2015**, *7*, 3997−4004.
(32) Salzemann, C.; Brioude, A.; Pileni, M. P. Tuning of Copper Nanocrystals Optical Properties with Their Shapes. *J. Phys. Chem. B* **2006**, *110*, 7208−7212.
(33) Chan, G. H.; Zhao, J.; Hicks, E. M.; Schatz, G. C.; Van Duyne, R. P. Plasmonic Properties of Copper Nanoparticles Fabricated by Nanosphere Lithography. *Nano Lett.* **2007**, *7*, 1947−1952.
(34) Bohren, C. F.; Huffman, D. R. *Absorption and Scattering of Light by Small Particles*; Wiley-VCH Verlag GmbH: Weinheim, Germany, 2008.
(35) Kang, B.; Ko, S.; Kim, J.; Yang, M. Microelectrode Fabrication by Laser Direct Curing of Tiny Nanoparticle Self-Generated from Organometallic Ink. *Opt. Express* **2011**, *19*, 2573−2579.
(36) Pile, D. ORGANIC ELECTRONICS: Laser-Induced Electrode Fabrication. *Nat. Photonics* **2011**, *5*, 199.
(37) Jeong, S.; Woo, K.; Kim, D.; Lim, S.; Kim, J. S.; Shin, H.; Xia, Y.; Moon, J. Controlling the Thickness of the Surface Oxide Layer on Cu Nanoparticles for the Fabrication of Conductive Structures by Ink-Jet Printing. *Adv. Funct. Mater.* **2008**, *18*, 679−686.
(38) Kim, D.; Moon, J. Highly Conductive Ink Jet Printed Films of Nanosilver Particles for Printable Electronics. *Electrochem. Solid-State Lett.* **2005**, *8*, J30−J33.
(39) Nge, T. T.; Nogi, M.; Suganuma, K. Electrical Functionality of Inkjet-Printed Silver Nanoparticle Conductive Tracks on Nanostructured Paper Compared with Those on Plastic Substrates. *J. Mater. Chem. C* **2013**, *1*, 5235−5243.
(40) Fuller, S. B.; Wilhelm, E. J.; Jacobson, J. M. Ink-Jet Printed Nanoparticle Microelectromechanical Systems. *J. Microelectromech. Syst.* **2002**, *11*, 54−60.
(41) Kang, B.; Yun, J.; Kim, S. G.; Yang, M. Adaptive Fabrication of a Flexible Electrode by Optically Self-Selected Interfacial Adhesion and Its Application to Highly Transparent and Conductive Film. *Small* **2013**, *9*, 2111−2118.

DOI: 10.1021/acs.chemmater.6b00013
Chem. Mater. 2016, 28, 4151−4159